


# Anomalous birefringence through metasurface-based cavities with linear-to-circular polarization conversion

Aofang Zhang and Rui Yang <sup>\*</sup>

*National Key Laboratory of Antennas and Microwave Technology, School of Electronic Engineering, Xidian University, Xi'an 710071, People's Republic of China*



(Received 26 May 2019; revised manuscript received 28 November 2019; published 19 December 2019)

We propose the metasurface-based cavities for splitting a linearly polarized (LP) electromagnetic wave into two symmetric circularly polarized (CP) beams with opposite helicities. More specifically, periodic strip slits and rectangular C-slits etched on substrate integrated waveguide cavities are shown to be capable of perfectly coupling the LP wave into the cavities from the strip slit array, and then releasing them with specific polarization directions according to the orientations of the C-slits. Such metasurface-based cavities with gradient oriented C-slit array would further create the opposite equivalent phase gradients for the right-hand and left-hand CP transmitting waves that are decomposed from the released LP wave with anomalous birefractions and polarization conversion simultaneously.

DOI: [10.1103/PhysRevB.100.245421](https://doi.org/10.1103/PhysRevB.100.245421)

## I. INTRODUCTION

The birefringence effects of light, usually observed from anisotropic materials in nature when electromagnetic (EM) fields are penetrating through, have been widely applied in the design of optical polarizing devices [1,2].

Metasurfaces with phase-modulated layouts of meta-atoms have recently demonstrated perfect dual beam generation with controllable traveling directions to mimic the birefringence in the reflection regime [3–6], where the isotropic metasurfaces can normally create dual beam reflections with the same polarizations of the original incidence [3,4], while the anisotropic metasurfaces would be able to produce two orthogonal linearly polarized (LP) components reflected in different directions [5,6]. In the meanwhile, the metasurfaces also demonstrate the great capabilities to tune the polarization states of the EM fields [7–16], where LP waves can be converted into circularly polarized (CP) waves through assigning the equal amplitudes and  $90^\circ$  phase difference to the two orthogonal LP components [10–16]. Especially, the metasurfaces have also been shown to be capable of manipulating the traveling directions of the reflections while converting the polarizations of the EM fields through tuning the amplitudes and phases of two orthogonal LP components simultaneously [14,15].

However, the investigations of tuning the polarizations and traveling directions of EM fields at the same time are mostly based on reflective metasurfaces with few studies consulting the transmissive metasurfaces, especially for the cases of linear-to-circular polarization transformation with controllable ray traces. This is because the transmittance of the phase-gradient transmissive metasurfaces usually varies with the change of transmitting phases and it is not trivial to obtain the desired refractions from such bifunctional interfaces when

compared with the metamirrors in the reflection regime. It would thus be more challenging to perform the conversion of LP into CP waves with controllable refraction angles with high transmission efficiency [16], as it requires the gradient phase discontinuities of two orthogonal polarized components of EM fields over the metasurfaces while maintaining the equal assignments of the amplitudes of such two orthogonal polarized fields with a fixed phase difference of  $90^\circ$ . Contemporary strategy through assembling Pancharatnam-Berry metaelements [17–26] with spatially varying axis orientations would fulfill such bifunctionalities of performing the polarization conversion while redirecting the refraction angles. Especially, metasurfaces based on the Pancharatnam-Berry method possess the benefits of fabrication-friendly ultrathin constructions with polarization sensitiveness, and scalability at optical frequency ranges. Investigations have verified the functionalities of Pancharatnam-Berry metasurfaces as qualified polarization converters [19–22], and beam collimating lenses [23–26]. However, it has also been proved that the transmission efficiency of cross-polarization conversion by a single layer metasurface is quite low with only 25% [17,19] of the theoretical upper limit. To overcome such a drawback, one can employ the multiple layered metasurface to acquire the  $2\pi$  range phase and nearly unit transmission, where fully controllable Pancharatnam-Berry metasurface array with high conversion efficiency would thus be available. We can observe from the present literature that using cascade metasurfaces in the transmission regime, normally with three [17] or four [18] layered constructions, would offer the desired high conversion efficiency of LP into CP waves with controllable refraction angles. However, these designs would unavoidably be loaded with an increased overall thickness at the cost of the high efficiency. Therefore, it is always appealing to transform the incoming light with satisfactory polarization conversion efficiency while retaining the benefits of thin profile constructions of the metasurfaces. With this end in view, we propose the

<sup>\*</sup>ruiyang.xidian@gmail.com

metasurface-based cavities to generate anomalous refractions of split dual beams with linear to circular polarization conversion with high transformation efficiency. Our design would not dramatically increase the overall thickness compared with the ultrathin single layered Pancharatnam-Berry metasurface, but, at the same time, can sufficiently increase the conversion efficiency through coupling of an incoming LP wave into a certain cavity mode and then reemitting as CP waves with user-defined transmission phases. More specifically, we show that the periodic strip slits and rectangular C-slits etched on substrate integrated waveguide (SIW) cavities would perfectly couple the LP wave into the cavities to form the resonant mode of  $TM_{110}$  through the gates of the slit array, and then release the transmitting waves with specific polarization directions according to the orientations of the C-slits. By introducing the gradient oriented C-slit array on such metasurface-based cavities, the opposite equivalent phase gradients would be readily created for the right-hand CP (RHCP) and left-hand CP (LHCP) transmitting waves that are decomposed from the released LP wave to achieve anomalous birefringence and polarization conversion simultaneously in the transmission regime.

## II. MODELING OF THE METASURFACE-BASED CAVITIES

Figure 1 illustrates the schematic diagram of the anomalous birefringence from the metasurface-based cavities with polarization conversion, where an LP wave is split into two orthogonal CP waves. Each unit cell of such a metasurface-based cavity consists of a strip slit etched on the back side and a rectangular C-slit etched on the front side of an SIW cavity formed by four rows of metallized cylindrical vias within a metal-coated dielectric substrate. The strip slit array is responsible for coupling the LP wave into the cavities, while different oriented C-slits induce anomalous birefringence through creating opposite equivalent phase gradients for the RHCP component and the LHCP component of the transmitting waves. In this way, the metasurface-based

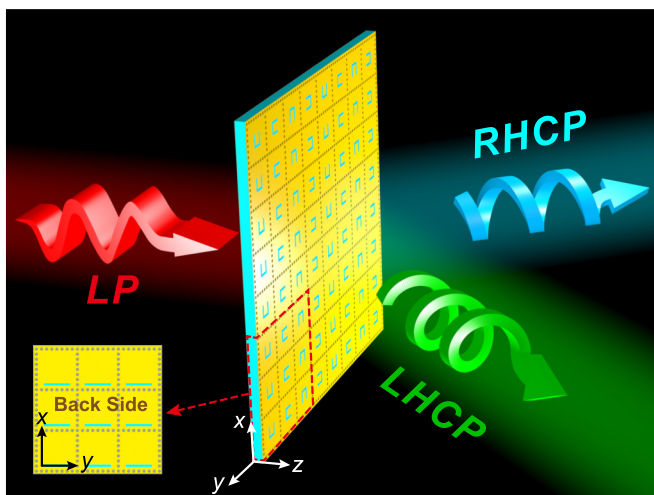


FIG. 1. Schematic diagram of the anomalous birefringence from the metasurface-based cavities with an LP wave splitting into an RHCP wave and an LHCP wave.

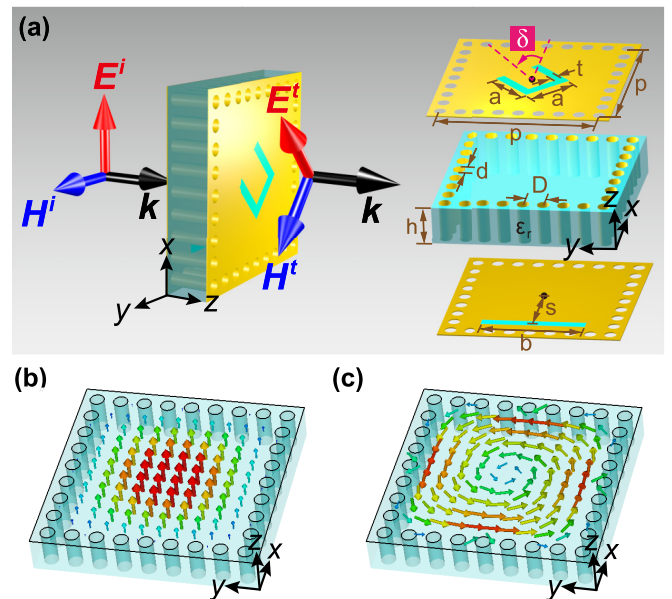


FIG. 2. Metasurface based cavity under the illumination of an  $x$ -polarized EM wave. (a) The configuration of the metasurface-based cavity, where the C-slit is demonstrated to have a rotating angle of  $\delta$ . (b) E-field vector and (c) H-field vector of the  $TM_{110}$  mode in the same structural SIW cavity with no etched slits.

cavities can thus split the incident LP wave into two orthogonal CP waves with opposite refraction angles.

Consider the metasurface-based cavity with the same and periodic unit cells under the illumination of an  $x$ -polarized wave  $\hat{x}E_x^i$ , as shown in Fig. 2(a), where the rectangular C-slits etched on the front side of the SIW cavity are set with a rotating angle of  $\delta$ . Such an SIW cavity should support resonant modes of  $TM_{mn0}$  ( $m = 1, 2, 3, \dots$  and  $n = 1, 2, 3, \dots$ ) and the relationship between the resonant frequency  $f_r$  and the cavity dimensions would be determined by  $f_r \approx c_0 \sqrt{m^2 + n^2} / (2\sqrt{\epsilon_r} p_{\text{eff}})$  with  $c_0$  of the light velocity and  $p_{\text{eff}} = p - d^2 / (0.95D)$  as the effective side length of the SIW cavity [9,27,28]. The resonant mode of  $TM_{110}$  can thus be excited in the SIW cavity by having the structural parameters of  $d = 0.6$  mm,  $D = 1.02$  mm,  $p = 8.16$  mm,  $h = 3$  mm,  $s = 3$  mm,  $t = 0.4$  mm, and  $\epsilon_r = 3.5$ . We can observe in Figs. 2(b) and 2(c) that the vector of E-field of the  $TM_{110}$  mode points in the  $z$  direction, while the vector of H field of the  $TM_{110}$  mode demonstrates the rotational symmetric distribution in the  $xy$  plane.

Figure 3 demonstrates the transmission characteristics of the metasurface-based cavities by imposing the boundary condition with the Floquet mode analysis that virtually repeats the modeled structure in Fig. 2(a) periodically in two directions. For the metasurface-based cavities, the strip slits couple the  $x$ -polarized wave into the cavities to form the resonant mode of  $TM_{110}$  and the C-slits then release the  $TM_{110}$  mode in the cavities as the transmitting wave  $\vec{E}^t$  with both  $x$ -polarized component  $E_x^t$  and  $y$ -polarized component  $E_y^t$  having the relationship of

$$\vec{E}^t = \hat{x}E_x^t + \hat{y}E_y^t = (\hat{x}T_{xx} + \hat{y}T_{yx})E_x^i, \quad (1)$$

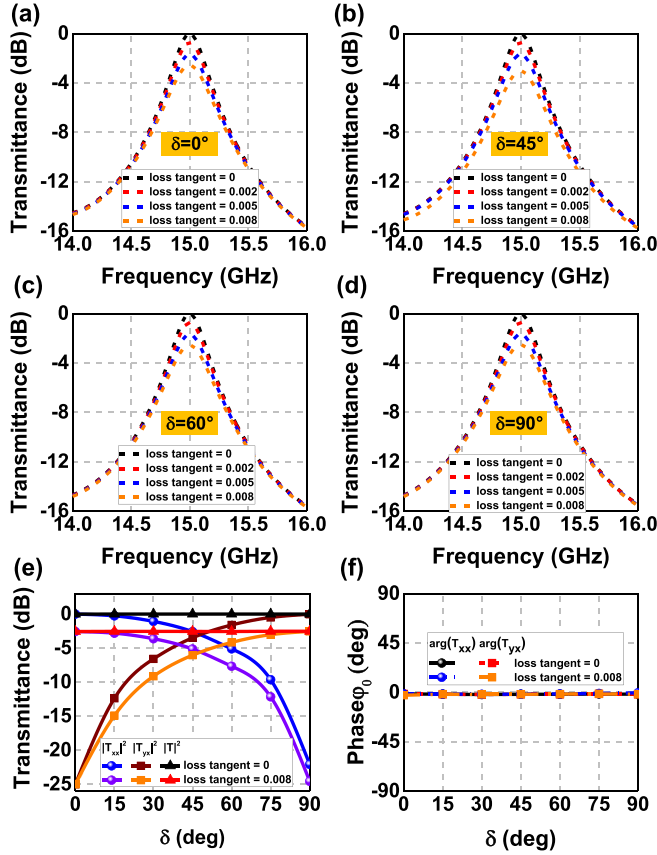


FIG. 3. Transmission characteristics of the metasurface-based cavities for the lossless and lossy cases at 15 GHz, where the slit parameters should be slightly adjusted to maintain the resonant transmissions when  $\delta$  is changing. (a) Transmittance varied with frequency when  $\delta = 0^\circ$ , where  $a = 2.63$  mm and  $b = 5.27$  mm. (b) Transmittance varied with frequency when  $\delta = 45^\circ$ , where  $a = 2.65$  mm and  $b = 5.33$  mm. (c) Transmittance varied with frequency when  $\delta = 60^\circ$ , where  $a = 2.67$  mm and  $b = 5.36$  mm. (d) Transmittance varied with frequency when  $\delta = 90^\circ$ , where  $a = 2.72$  mm and  $b = 5.48$  mm. (e) Transmittance and (f) transmission phase  $\varphi_0$  varied with  $\delta$  at 15 GHz.

where  $T_{xx}$  and  $T_{yx}$  refer to the linear transmission coefficients in the  $x$  and  $y$  directions, respectively. We can observe in Figs. 3(a)–3(d) that the metasurface-based cavities could possess perfect 100% transmittance at 15 GHz for the lossless case, and the transmittance of the periodic unit cell would gradually decrease as the loss tangent of the dielectric increases. However, the transmittance can still maintain a constant value regardless of the variation of the C-slit orientations with  $|T|^2 = |T_{xx}|^2 + |T_{yx}|^2$  in Fig. 3(e), although suffering with dielectric losses. The  $x$ - and  $y$ -polarized components would decrease and increase respectively when we enlarge the C-slit rotating angle of  $\delta$ . On the other hand, the transmission phase of  $\varphi_0 \approx 0^\circ$  can almost keep unchanged at 15 GHz despite the variations of  $\delta$  with and without the dielectric losses, as shown in Fig. 3(f). Clearly, the transmitting fields would still maintain the LP waves, and the polarization direction should be in accord with the rotating angle of the C-slits, as the transmission coefficients in the  $x$  and  $y$  directions can be

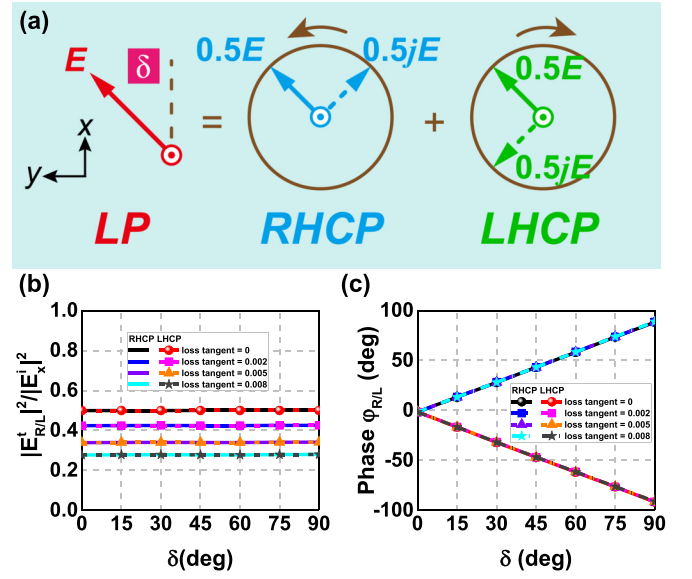


FIG. 4. Characteristics of the equivalent CP waves for the lossless and lossy cases. (a) Relationship between LP wave and CP waves. (b) Equivalent transmittances and (c) transmission phases of the CP waves varied with  $\delta$  at 15 GHz.

approximated as

$$T_{xx} \approx |T| \cos \delta e^{j\varphi_0}, \quad (2)$$

$$T_{yx} \approx |T| \sin \delta e^{j\varphi_0}. \quad (3)$$

The physical mechanism behind such a phenomenon is that the C-slit resonator can only be effectively excited by the H-field vector perpendicular to the opening gap of the C-slit. Therefore, different orientated C-slits would have the same excitation status as the  $TM_{110}$  mode possessing the rotational symmetric H-field distribution, and the polarization direction of the transmitting wave would be rotated according to the orientation of the C-slits.

We understand that an arbitrarily transmitting LP wave  $\vec{E}^t$  can be equivalent to the combination of the RHCP component  $E_R^t$  and the LHCP component  $E_L^t$ , as shown in Fig. 4(a) with the expression of

$$\vec{E}^t = \hat{R}E_R^t + \hat{L}E_L^t, \quad (4)$$

where  $\hat{R} = (\hat{x} - j\hat{y})/\sqrt{2}$  and  $\hat{L} = (\hat{x} + j\hat{y})/\sqrt{2}$  refer to the RHCP unitary vector and LHCP unitary vector, respectively. Therefore, by solving Eqs. (1)–(4) we can obtain

$$E_R^t = \frac{1}{\sqrt{2}}|T|E_x^i e^{j(\delta+\varphi_0)}, \quad (5)$$

$$E_L^t = \frac{1}{\sqrt{2}}|T|E_x^i e^{j(-\delta+\varphi_0)}. \quad (6)$$

Clearly, the transmittances  $|E_{R/L}^t|^2/|E_x^i|^2$  of both RHCP and LHCP components should possess equal values of total transmission, and the transmission phases of the RHCP and the LHCP components would be  $\varphi_R = \delta + \varphi_0$  and  $\varphi_L = -\delta + \varphi_0$ , respectively. Figures 4(b) and 4(c) demonstrate the equivalent transmission characteristics of the RHCP and LHCP components at 15 GHz. We can observe in Fig. 4(b) that

both of the RHCP and LHCP components would own half of the transmitting energy in the lossless case, regardless the variations of  $\delta$ . On the other hand, the lossy dielectrics degrade the overall transmissions; however, the RHCP and LHCP components would decay in the same manner and can still maintain identical amplitude. In addition, we can also observe in Fig. 4(c) that  $\varphi_R$  and  $\varphi_L$  of RHCP and LHCP components would achieve the same absolute values of transmission phases with opposite gradients when  $\delta$  is changing in both cases with and without the dielectric losses. Therefore, we can utilize the metasurface-based cavities with gradient oriented C-slit array to create the opposite equivalent phase gradients of the two CP components according to the generalized Snell's law of refraction to split the RHCP and the LHCP waves, where the rotating angle gradient of the C-slits is set as  $d\delta/dy = d\varphi_R/dy = -d\varphi_L/dy = -k_0 \sin \theta$  with  $k_0$  referring to the wave number in free space [29–32]. And in this way, we can thus realize anomalous birefringence and polarization conversion simultaneously by transforming the incident LP wave to the RHCP and LHCP waves.

We now use the metasurface-based cavities with gradient oriented C-slit array to create the opposite equivalent phase gradients of two orthogonal CP components, and split two such CP waves with the opposite refraction angles of  $\pm\theta$ . For instance, when the orientation gradients of the C-slits between the adjacent unit cells is set as  $90^\circ$  in the  $y$  direction as shown in Fig. 1(a), we would obtain  $d\varphi_R/dy = -0.61k_0$  with the refraction angle of  $-38^\circ$  for the RHCP component and  $d\varphi_L/dy = 0.61k_0$  with the refraction angle of  $38^\circ$  for the LHCP component. Figures 5(a) and 5(b) demonstrate the E-field distributions and 3D far-field performances of such metasurface-based cavities under the incidence of an  $x$ -polarized wave. Figure 5 thus demonstrates the simulation results of such anomalous birefringence with polarization conversions through metasurface-based cavities, where an  $x$ -polarized plane wave is employed as the illumination. The metasurface-based cavities in the simulation are assumed lossless with periodic boundary conditions. We can observe in Fig. 5(a) that the metasurface-based cavities could be able to function as an EM beam splitter to split the incident LP wave to two beams and in Fig. 5(b) that the RHCP component is steering in the direction of  $-38^\circ$  while the LHCP component would propagate in the opposite direction of  $38^\circ$  as we expected, which achieves the anomalous birefringences with polarization conversion from the LP wave to both RHCP and LHCP waves. Clearly, the beam refraction directions can also be controlled by using different rotating angle gradients, as shown in Figs. 5(c)–5(f). We can observe that the refraction directions would be  $\pm 18^\circ$ ,  $\pm 24^\circ$ ,  $\pm 38^\circ$ , and  $\pm 54^\circ$  when the orientation gradients between the adjacent unit cells are  $45^\circ$ ,  $60^\circ$ ,  $90^\circ$ , and  $120^\circ$ , respectively. Clearly, the proposed metasurface-based cavity can possess perfect transmittance in the ideal lossless case. The far-field radiations would experience some degradations with approximate 0.7 dB, 1.6 dB, and 2.6 dB, respectively, when we employ the lossy dielectric with the loss tangents of 0.002, 0.005, and 0.008. However, the directions of the split beams can keep almost unchanged regardless the dielectric loss. On the other hand, the polarization states of the split beams can be quantified by the linear to circular polarization conversion ratio [33,34]

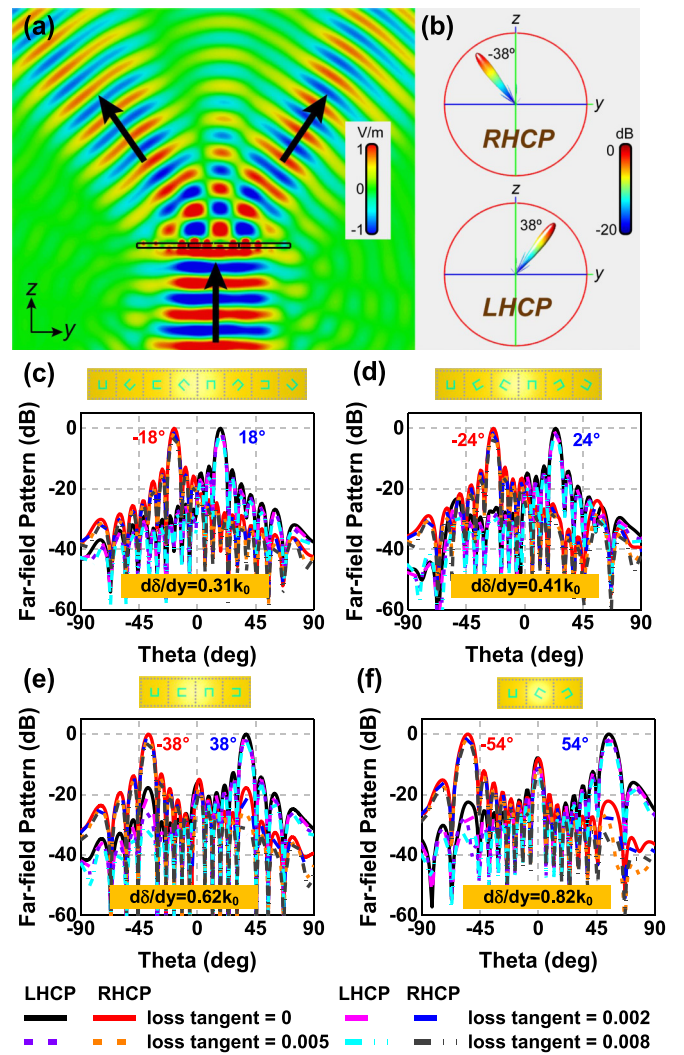


FIG. 5. Anomalous birefringence with polarization conversions through metasurface-based cavities for the lossless and lossy cases when under the illumination of an  $x$ -polarized wave at 15 GHz. The slit parameters are  $a = 2.78$  mm and  $b = 5.65$  mm for  $\delta = 120^\circ$ ,  $a = 2.82$  mm and  $b = 5.72$  mm for  $\delta = 135^\circ$ ,  $a = 2.90$  mm and  $b = 5.82$  mm for  $\delta = 180^\circ$ , and other structural parameters are the same as in Fig. 3. Due to the symmetry of the metasurface-based cavities, the values of  $a$  and  $b$  are the same as  $360^\circ - \delta$  when  $\delta$  is changing from  $180^\circ$  to  $360^\circ$ . (a) Normalized E-field distributions with  $E_x$  component. (b) Normalized 3D far-field patterns. In (a) and (b), the orientation gradients of the C-slits between the adjacent unit cells are  $90^\circ$ , and the E-fields are normalized by 600 V/m and the radiation patterns are normalized by  $14.5$  dBW/m $^2$ . (c)–(f) Normalized far-field intensities in  $yz$  plane with different  $d\delta/dy$ , where the orientation gradients of the C-slits between the adjacent unit cells are  $45^\circ$ ,  $60^\circ$ ,  $90^\circ$ , and  $120^\circ$ , respectively.

$\eta_{cp} = \frac{||E_L|^2 - |E_R|^2|}{(|E_L|^2 + |E_R|^2)}$ , where  $E_R$  and  $E_L$  refer to the electric amplitude of RHCP and LHCP components, respectively. Clearly, the definition of  $\eta_{cp}$  only indicates the purity of the circular polarization of the transmitting waves in the propagating directions and would thus not suffer with the dielectric losses. As a result,  $\eta_{cp}$  would be 99.9%, 99.6%, 96.7%, and 98.8% at the refraction

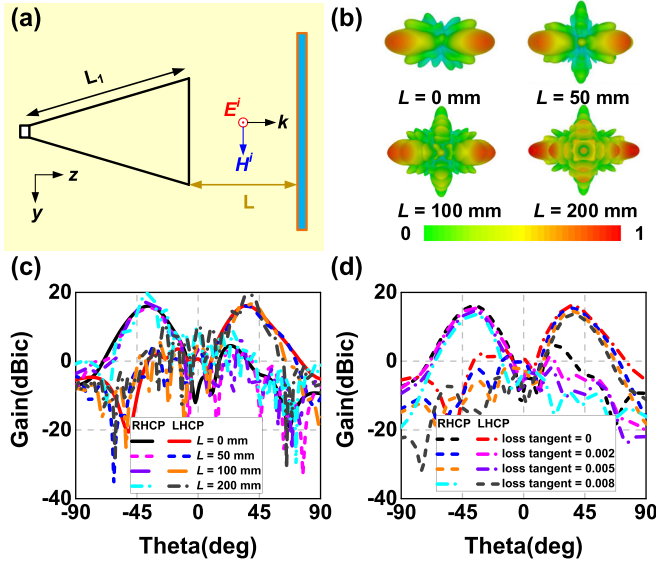


FIG. 6. Simulation results of horn fed metasurface-based cavity with  $d\delta/dy = 0.61k_0$ . (a) Practical implementation of the LP plane wave illuminating on the metasurface-based cavities and normalized E-filed distribution of the rectangular horn antenna. The aperture sizes of the rectangular horn antenna are 70 mm and 90 mm in the  $x$  and  $y$  directions with  $L_1 = 120$  mm. The metasurface-based cavity is having the aperture of  $130.56 \text{ mm} \times 130.56 \text{ mm}$ . (b) Normalized 3D far-field patterns and (c) 2D far-field patterns in  $yz$  plane of the horn fed metasurface-based cavity with different separation distances  $L$ . (d) Simulation results of the horn fed metasurface-based cavity with different loss tangents, where the metasurfaces are set closely on the horn exit with  $L = 0$  mm.

angles when  $d\delta/dy = 0.31k_0$ ,  $d\delta/dy = 0.41k_0$ ,  $d\delta/dy = 0.61k_0$ , and  $d\delta/dy = 0.82k_0$ , respectively, demonstrating efficient conversions from linear polarizations to circular polarizations.

### III. IMPLEMENTATION OF THE METASURFACE-BASED CAVITIES

In order to verify the anomalous birefringence with linear to circular polarization conversion, we load the metasurface-based cavities on a wide aperture rectangular horn antenna. The horn antenna acts as the emitter of the  $x$ -polarized plane wave and can be readily implemented in the measurement. Figure 6 thus demonstrates the far-field performances with different separation distances  $L$  between the horn antenna and the metasurface-based cavities. We can observe that the metasurface-based cavities could all effectively split the incident wave emitted by the horn antenna into two orthogonal CP beams with different  $L$ . However, the side lobes of the released fields gradually increase as the distance gets further and reach a very high level when the separation distance is 200 mm. The reason is that large parts of the radiations from the horn antenna would simply go around the metasurface-based cavity when we enlarge the separation distance, thus producing higher side lobes. On the other hand, the one with metasurface-based cavities closely at the location of the horn exit achieves very sound radiation performance as we expected. We continue to investigate the loss effects on

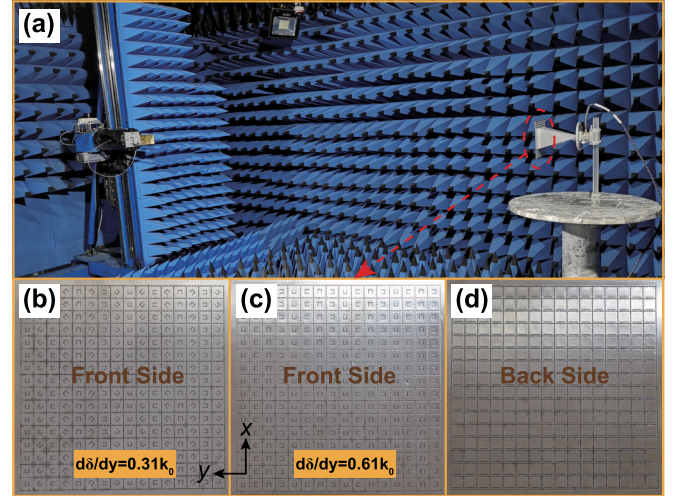


FIG. 7. Experimental setup and manufactured photos of the metasurface-based cavities. (a) Experimental setup. The horn antenna is the same as the one in Fig. 6. (b)–(d) Manufactured photos of the metasurface-based cavities. The aperture size of the metasurface-based cavity is the same as the one in Fig. 6 with  $130.56 \text{ mm} \times 130.56 \text{ mm}$ .

the performance of the metasurface-based cavities, where the metasurfaces in such investigations are thus set closely on the horn exit with  $L = 0$  mm. We can observe that the gain values of anomalous birefringence decrease gradually as the loss tangents of the metasurface-based cavities are enlarged. However, the overall functionalities of the simultaneous tuning of propagating directions of CP waves and LP-to-CP conversion are still valid.

Finally, we fabricate the proposed metasurface-based cavities with two different C-slit orientation gradients  $d\delta/dy =$

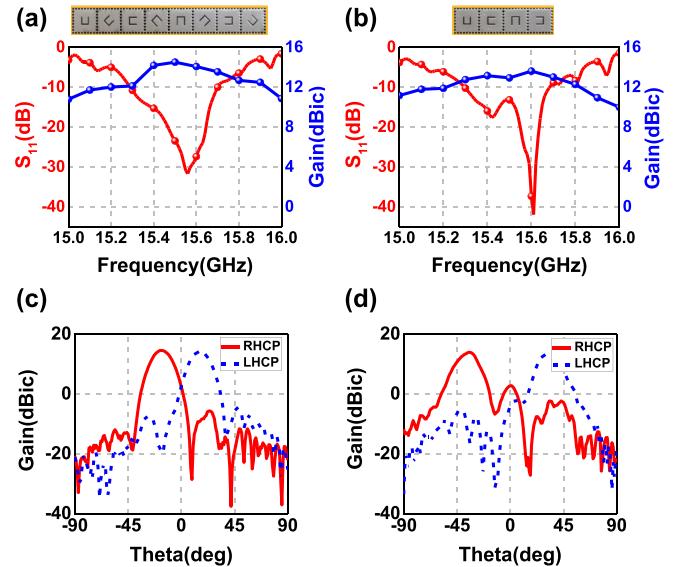


FIG. 8. Measured results of the metasurface-based cavities. (a), (b) Reflection coefficients of the horn fed metasurface-based cavities and gains in  $yz$  plane with different  $d\delta/dy$ . (c) Measured far-field patterns at 15.5 GHz when  $d\delta/dy = 0.31k_0$ . (d) Measured far-field patterns at 15.6 GHz when  $d\delta/dy = 0.61k_0$ .

$0.31k_0$  and  $d\delta/dy = 0.61k_0$  as demonstrated in Fig. 7. In the experiment, the F4B circuit board ( $\epsilon_r = 3.5$ ; loss tangent = 0.0015) is chosen as the dielectric substrate and loaded on the horn antenna as demonstrated in Fig. 7. The radiation performances are tested by using an antenna measurement system in the microwave chamber, where we place the whole system in the center of the turret to test the gain when the turret rotates  $360^\circ$  and the radiation patterns are obtained by comparing with a standard diagonal horn. Figure 8 demonstrates the experimental results of the metasurface-based cavities. We can observe that the operating bandwidth of the proposed design is very limited due to inherent resonant behaviors of the metasurface-based cavity and the center frequencies shift about 0.5 GHz and 0.6 GHz respectively of the measured results as demonstrated in the S parameters and gains with different  $d\delta/dy$ , as shown in Figs. 8(a) and 8(b). In the simulation, we can slightly adjust slit parameters to maintain the resonant transmissions at 15 GHz as shown in Fig. 3, while in the experiments such frequency shifts mainly come from the fabrication tolerance of smaller permittivity of the dielectric substrate and slit apertures during the practical implementation. We can also observe that the RHCP and LHCP waves propagate in the opposite directions as we expected

with the refraction angles in Figs. 8(c) and 8(d). In addition, the polarization conversion ratios are shown to be 99.9% and 97.6% at the refraction angles, respectively.

#### IV. CONCLUSIONS

In conclusion, we have proposed the metasurface-based cavities for the anomalous birefringence by transforming an LP wave into two CP waves with opposite helicities simultaneously in this paper. Especially, we show that the periodic strip slits and gradient orientated C-slits etched on SIW cavities could perfectly couple the LP wave into the cavities, and release them with opposite refraction angles for the RHCP and LHCP waves. Our design of building up birefringent metasurface-based cavities should pave the way for the development of more advanced polarizing devices.

#### ACKNOWLEDGMENTS

This work was supported by the National Natural Science Foundation of China (Grants No. 61671344 and No. 61301072).

- 
- [1] S.-T. Wu, *Phys. Rev. A* **33**, 1270 (1986).
- [2] S. Bardal, A. Kamal, and P. S. J. Russell, *Opt. Lett.* **17**, 411 (1992).
- [3] X. Zhang, R. Deng, Y. Fan, C. Jiang, and M. Li, *ACS Photon.* **5**, 2997 (2018).
- [4] J.-S. Li, Z.-J. Zhao, and J.-Q. Yao, *Opt. Express* **25**, 29983 (2017).
- [5] T. Cai, S. W. Tang, G. M. Wang, H. X. Xu, and L. Zhou, *Adv. Opt. Mater.* **5**, 1600506 (2016).
- [6] S. Liu, T. J. Cui, X. Quan, B. Di, L. Du, W. Xiang, X. T. Wen, C. Ouyang, Y. Z. Xiao, and Y. Hao, *Light: Sci. Appl.* **5**, e16076 (2016).
- [7] N. K. Grady, J. E. Heyes, D. R. Chowdhury, Y. Zeng, M. T. Reiten, A. K. Azad, A. J. Taylor, D. A. R. Dalvit, and H.-T. Chen, *Science* **340**, 1304 (2013).
- [8] C. Pfeiffer, C. Zhang, V. Ray, L. J. Guo, and A. Grbic, *Optica* **3**, 427 (2016).
- [9] S. A. Winkler, W. Hong, M. Bozzi, and K. Wu, *IEEE Trans. Antennas Propag.* **58**, 1202 (2010).
- [10] M. Pu, P. Chen, Y. Wang, Z. Zhao, H. Cheng, C. Wang, X. Ma, and X. Luo, *Appl. Phys. Lett.* **102**, 131906 (2013).
- [11] J. D. Baena, J. P. del Risco, A. P. Slobozhanyuk, S. B. Glybovski, and P. A. Belov, *Phys. Rev. B* **92**, 245413 (2015).
- [12] J. K. Gansel, T. Michael, M. S. Rill, D. Manuel, B. Klaus, S. Volker, V. F. Georg, L. Stefan, and W. Martin, *Science* **325**, 1513 (2009).
- [13] H. L. Zhu, S. W. Cheung, K. L. Chung, and T. I. Yuk, *IEEE Trans. Antennas Propag.* **61**, 4615 (2013).
- [14] A. Zhang and R. Yang, *Appl. Phys. Lett.* **113**, 091603 (2018).
- [15] S. C. Jiang, X. Xiong, Y. S. Hu, S. W. Jiang, Y. H. Hu, D. H. Xu, R. W. Peng, and M. Wang, *Phys. Rev. B* **91**, 125421 (2015).
- [16] N. Yu, F. Aieta, P. Genevet, M. A. Kats, Z. Gaburro, and F. Capasso, *Nano Lett.* **12**, 6328 (2012).
- [17] C. Liu, Y. Bai, Q. Zhao, Y. Yang, H. Chen, J. Zhou, and L. Qiao, *Sci. Rep.* **6**, 34819 (2016).
- [18] W. Luo, S. Sun, H.-X. Xu, Q. He, and L. Zhou, *Phys. Rev. Appl.* **7**, 044033 (2017).
- [19] X. Ding, F. Monticone, K. Zhang, L. Zhang, D. Gao, S. N. Burokur, A. de Lustrac, Q. Wu, C.-W. Qiu, and A. Alù, *Adv. Mater.* **27**, 1195 (2015).
- [20] L. Jianxiong, C. Shuqi, Y. Haifang, L. Junjie, Y. Ping, C. Hua, G. Changzhi, C. Hou-Tong, and T. Jianguo, *Adv. Funct. Mater.* **25**, 704 (2015).
- [21] L. Siqi, W. Guoxi, L. Xingyi, L. Mulong, G. Zhiqiang, Z. Lingxuan, Z. Chao, W. Leiran, S. Qibing, Z. Wei, and Z. Wenfu, *Appl. Phys. Express* **11**, 105201 (2018).
- [22] R. Xie, G. Zhai, X. Wang, D. Zhang, L. Si, H. Zhang, and J. Ding, *Adv. Opt. Mater.* **7**, 1900594 (2019).
- [23] T. Cai, G.-M. Wang, H.-X. Xu, S.-W. Tang, H. Li, J.-G. Liang, and Y.-Q. Zhuang, *Ann. Phys.* **530**, 1700321 (2017).
- [24] Z. Tao, X. Jianghao, L. Yun-Han, and W. Shin-Tson, *Opt. Express* **26**, 35026 (2018).
- [25] G. Ninghui, D. Zhang, R. Mengxin, W. Wei, C. Wei, Z. Xinzheng, and X. Jingjun, *Appl. Phys. Lett.* **113**, 113103 (2018).
- [26] L. Dianmin, F. Pengyu, E. Hasman, and L. B. Mark, *Science* **345**, 298 (2014).
- [27] L. Z. Yu, H. Wei, W. Ke, X. C. Ji, and J. T. Hong, *IEEE Trans. Microwave Theory Technol.* **53**, 1280 (2005).
- [28] C. H. Zhang, H. Wei, P. C. Xiao, X. C. Ji, W. Ke, and T. J. Cui, *IEEE Microwave Wireless Compon. Lett.* **15**, 95 (2005).
- [29] N. Yu, P. Genevet, M. A. Kats, F. Aieta, J.-P. Tetienne, F. Capasso, and Z. Gaburro, *Science* **334**, 333 (2011).

- [30] X. Zhang, Z. Tian, W. Yue, G. Jianqiang, Z. Shuang, H. Jiaguang, and Z. Weili, *Adv. Mater.* **25**, 4567 (2013).
- [31] S. Sun, K.-Y. Yang, C.-M. Wang, J. Ta-Ko, C. Wei Ting, L. Chun Yen, H. Qiong, X. Shiyi, K. Wen-Ting, and G. Guang-Yu, *Nano Lett.* **12**, 6223 (2012).
- [32] A. Díazrubio, V. S. Asadchy, A. Elsakka, and S. A. Tretyakov, *Sci. Adv.* **3**, e1602714 (2017).
- [33] J. Wang, Z. Shen, W. Wu, and K. Feng, *Opt. Express* **23**, 12533 (2015).
- [34] M. Mutlu, A. E. Akosman, and E. Ozbay, *Opt. Lett.* **37**, 2094 (2012).